Multibody System Dynamics
https://doi.org/10.1007/s11044-023-09899-4

RESEARCH

Identification of lumped stiffness parameters for a motorcycle model in investigating weave and wobble

Francesco Passigato[1] · Alexander Schramm[2] · Frank Diermeyer[1] · Silvio Sorrentino[2] · Achim Gordner[3] · Alessandro De Felice[2]

Received: 30 August 2022 / Accepted: 15 March 2023

Abstract
In motorcycle dynamics, great importance is attributed to the study of the weave and wobble vibration modes and, in particular, to the effects of the flexibility of structural components on their stability. Therefore, appropriate motorcycle models for studying weave and wobble should include flexible elements for describing the flexural behavior of components such as the main frame, front assembly, and rear swingarm. Different approaches are possible for modeling flexibilities: the most common among them are the lumped stiffness and the flexible multibody approaches. While the latter certainly provides higher accuracy, the former has advantages in terms of computational load, but, above all, it makes it easier to understand in the design phase how technical parameters, such as torsional and bending stiffness of a given structural component, can influence the stability of weave and wobble. The accuracy of lumped stiffness models strongly depends on parameter identification. In this study, a general method is proposed to determine appropriate lumped stiffness parameters for any given motorcycle component. The proposed method is tested and validated by comparing the weave and wobble modal behavior with the results of flexible multibody analysis. The lumped stiffness model is then adopted to carry out a sensitivity analysis aimed at identifying the effects on the weave and wobble stability of the torsional and bending stiffness of specific structural components of the motorcycle to optimize their design.

Keywords Parameter identification · Lumped stiffness · Weave · Wobble · Motorcycle dynamics · Stability analysis

1 Introduction

Weave and wobble are well-known eigenmodes of motorcycles, both involving lateral dynamics. The weave eigenvector is dominated by roll, yaw, and steering head rotation [1]

✉ F. Passigato
francesco.passigato@tum.de

1 Institute of Automotive Technology, TUM School of Engineering and Design, Technical University of Munich, Boltzmannstrasse 15, Garching, 85748, Germany

2 Department of Engineering Enzo Ferrari, University of Modena and Reggio Emilia, Via Pietro Vivarelli 10, Modena, 41125, Italy

3 BMW Group, Munich, Germany

Published online: 30 March 2023

with an eigenfrequency in the range 1-4 Hz [2]. Wobble is characterized mainly by steering head rotation, and its eigenfrequency varies from 6 to 10 Hz [3]. The stability of these eigenmodes is a safety critical problem because the motion caused by an unstable weave or wobble is not controllable by the rider and would likely lead to an accident. For this reason, weave and wobble have been extensively studied in the literature, with the first works dating back to the 1970s [4]. A deciding step in modeling weave and wobble was made when the flexibility of the structural components was included in the models. In fact, particularly for wobble, this step allowed the correct prediction of the change of mode damping with speed [5–8].

For modeling the stiffness of structural components, different approaches are possible: the most used and simple is the lumped stiffness approach. It consists of representing the flexibility of a component with a single parameter, i.e., a concentrated stiffness, see Sect. 2. The second approach is the Elastic Multibody Simulation (EMBS) [9], where the classical formulation of multibody simulation is extended to include flexible bodies. In this case, the flexibility is represented as a distributed property so that the real deformation is better approximated. The lumped stiffness approach is attractive for its limited modeling effort, short computational time, and, above all, because it makes it easier to understand in the design phase how technical parameters, such as the torsional and bending stiffness of a given structural component, can influence stability. However, the strong approximation of the actual flexural behavior, which is intrinsic in this method, may negatively affect the accuracy when modeling weave and wobble.

The crucial part of the lumped stiffness approach is the identification of the parameters [10]. In the literature, most models using the lumped stiffness approach make assumptions about the position of the joints for modeling flexibility. However, as shown in [11], these assumptions may lead to inaccurate results when studying weave and wobble.

This paper presents a method for parameterizing a lumped stiffness model of any structural component. It is based on the identification of the deformation axis of each component and can be applied to real components or using a simulation environment, as in the present paper. The method is applied to each structural component of a motorcycle, and the obtained lumped stiffness model is compared to a flexible multibody model in the simulation of weave and wobble. The decision to use the lumped stiffness approach for studying the effect of structural flexibilities on weave and wobble is justified by the necessity of obtaining stiffness values with a physical meaning that can be easily interpreted and adapted. In fact, the developed lumped stiffness model lends itself to carrying out a sensitivity analysis to understand, for every component, if its torsional or bending stiffness is more important for the stability of weave and wobble. The results of the sensitivity analysis can help to optimize the stiffness in the early design phase of structural components so that the overall weight can be minimized while ensuring the stability of weave and wobble.

2 State of the art

As mentioned in the introduction, structural flexibility is important to the stability of weave and wobble. The first works modeling the flexibility of structural components for the study of weave and wobble are [5, 6]. They use two different approaches to model the flexibility at the front of the motorcycle. The authors of [5] model the frame torsional flexibility with a revolute joint and a coaxial rotational spring/damper at the steering head joint with its rotation axis perpendicular to the fork axis. In [6], the bending flexibility of the front fork is modeled with a revolute joint and a coaxial rotational spring/damper along the fork with

its rotation axis perpendicular to the fork axis. The aim is mainly to investigate the effect of this stiffness on weave and wobble and not to exactly reproduce the fork deformation. For this reason, the position of the revolute joint and the stiffness value are not based on real measurement but are varied to draw information about a possible optimized design. Based on this first experience, other works followed in its stead, by adopting the lumped stiffness approach for modeling the flexibility of structural components. In [12], the approaches in [5, 6] are combined, and the stiffness values are derived from real measurements, still maintaining the assumptions on the position and orientation of the revolute joints. The author of [13] proposes an analysis where the position of the deformation axis of the frame is varied and the effect on weave and wobble investigated. These modeling approaches, where the position of the joint and the value of the lumped stiffnesses is assumed or estimated, can be found in several other works, e.g., the works based on the model developed in [5], see, e.g., [14–19], or in independent works from other authors [7, 20].

The first attempt to parameterize a lumped stiffness model with a consistent procedure is found in [21, 22] for the front fork and in [23] for the swingarm. In [21], a procedure is developed where, using the mass properties and the bending eigenfrequency measured with experimental test, a lumped stiffness model is developed for the front fork bending flexibility. However, the orientation of the revolute joint axis is assumed to be perpendicular to the fork axis. The authors of [22, 23] identify the deformation axis of the structural component with either static or dynamic excitation. Dynamic excitation with a frequency equal to the first bending and torsional eigenfrequencies allows the identification of the bending and torsion axis, while the static test identifies the so-called twist axis, and the resulting deformation is generally a combination of bending and torsion. The authors provide different lumped stiffness models for the fork and swingarm, using the parameters identified through static or dynamic tests or a combination of the two. The weave and wobble eigenmodes are simulated with these models and compared to the rigid body case. However, the question remains about which combination provides the most realistic results. A similar approach was proposed in [24] for identifying the twist, bending, and torsion axes of a frame. However, no lumped stiffness model was parameterized with the resulting data.

The present paper answers the remaining open questions. In particular, the most suitable test for parameterizing a lumped stiffness model to study the influence of flexibilities on weave and wobble is identified. For that, a comparison with flexible multibody models is presented, which are considered the "ground truth". This way, it is demonstrated that the common assumptions on the location of the revolute joints to model the different flexibilities do not always lead to correct results.

Moreover, a sensitivity analysis will be carried out to separate the effect of bending and torsional flexibility of each component in the study of weave and wobble. Other works have already used this method to identify the most relevant parameters for motorcycle stability [25–27]. The common procedure is to calculate the analysis of variance (ANOVA) with a full factorial design of experiments. The results provide information on whether the varied factors interact with each other or only the main effects may be considered. In the latter case, a statistical model without interactions can be adopted [25]; in particular, a linear correlation technique (Pearson correlation coefficients) is used. More information about the sensitivity analysis is provided in Sect. 4.3.

3 Aim of the paper

The present paper is focused on two contributions. The first is the development of a unified procedure for parameterizing lumped stiffness models of the main structural components of

motorcycles. Attention is devoted to correctly reproducing the effect of structural flexibilities on weave and wobble with the lumped stiffness model. In particular, a test procedure is identified that allows the best approximation of a flexible multibody model with the lumped stiffness approach. The decision to use the lumped stiffness approach instead of leveraging on more advanced techniques for model condensation (e.g., dynamic condensation) is motivated by the necessity of identifying technical parameters that define the stiffness of each structural component. Then, in contrast to lumped stiffness models, condensation methods do not provide any physical parameters, which the engineer can directly interpret to derive an optimized design. Moreover, when applying condensation methods to the mechanisms of the front assembly and swingarm, it has to be determined at which level to apply the condensation. If it is applied to the whole assembly, composed of different bodies, the problem is preserving the kinematics of the mechanism itself. If condensation is applied to the single bodies of each assembly, further analysis will provide indications about the effects of the stiffness of single bodies, thus failing to analyze the effect of the stiffness of the whole assembly, which makes it difficult to derive information for an optimized design. The obtained lumped stiffness models are particularly useful for the second main contribution of this paper, i.e., a sensitivity analysis with the lumped stiffness model to study the separated effect on weave and wobble of bending and torsional flexibility for each structural component.

4 Methods

In this section, the methods used in this paper are presented. Section 4.1 briefly describes the motorcycle model used to generate the results. Section 4.2 provides details on the methods for the parameterization of lumped stiffness models. Section 4.3 summarizes the steps needed to conduct a sensitivity analysis with the motorcycle model and to calculate the stability index and correlation coefficients.

4.1 Motorcycle model

The motorcycle model is based on [11]. The motorcycle weighs 250 kg and is loaded with a rider (88 kg), two side bags and one top bag (40 kg in total). The front suspension is multilink with one longitudinal arm, while the rear suspension is of the four-bar link type swingarm. The Pacejka Magic Formula (MF) is used to model the tire forces [28]. A single contact point is assumed, and the tire thickness is accounted for. The kinematics of the contact point is based on the approach described in [8], where the relative orientation between the wheel carrier and ground is used to determine the reference system of the contact point.

In this work, two different versions of the motorcycle model are presented: one version uses EMBS with flexible bodies and is identical to that in [11]. The structural components modeled as flexible bodies are the frame, connected to a rigid engine, the front assembly, composed of the fork bridge, two stanchions, longitudinal arm and lower fork, and the swingarm, composed of lower link, upper link and wheel carrier. In the present work, this version is compared to a model of the same motorcycle that uses only rigid bodies and the lumped stiffness approach for representing the flexibilities. The parameters for the lumped stiffness models are identified with the method presented in Sect. 4.2. The theory of EMBS for modeling flexible bodies is explained in [11]. More information about the flexible multibody models is provided in the appendix.

With reference to Fig. 1, first, the model without flexibilities is described. It is composed of the following subsystems, bodies, and degrees of freedom (DOFs):

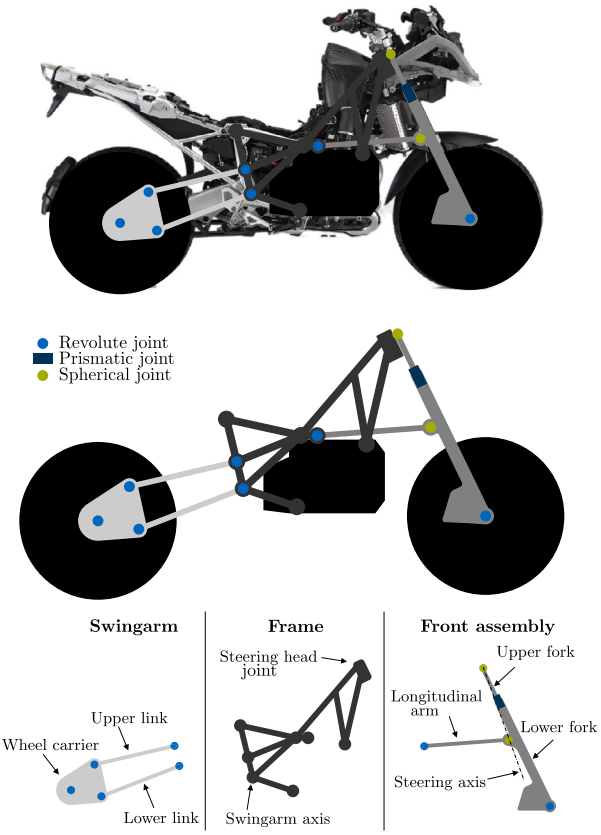

Fig. 1 Schematic representation of the motorcycle and its sub-assemblies. The image of the real motorcycle has been taken with permission from [29]

- *Main frame* of the motorcycle (including engine, fuel tank, and part of the driveline); it is constituted by a single rigid body, with 6 DOFs in 3D space (3 translations and 3 rotations about the inertial axes of the body).
- *Driver*, modeled as an additional rigid body split into two parts (not shown in Fig. 1): lower body fixed with respect to the main frame and upper body with one DOF of relative rotation with respect to the lower body, describing the rider's passive lean motion.
- *Front assembly*, composed of 3 rigid bodies: upper fork, including handlebars, lower fork, including wheel carrier, and longitudinal arm. Kinematically, the front assembly has 2 DOFs of relative motion with respect to the main frame; the first DOF is a rotation about the steering axis; the second one, for a fixed steering angle, is represented by a planar motion of the 3 members of the subsystem, yielding the front suspension travel. This can be inferred from Fig. 1, where the front assembly can be visualized as a spatial mechanism with 3 moving members with respect to the main frame, connected by one revolute joint, one prismatic joint, and two spherical joints (one placed at the steering head, the other one placed at the connection between longitudinal arm and lower steering assembly; the centers of these two spherical joints identify the position of the steering axis).
- *Front wheel*, including all rotating elements with the front wheel, modeled as a single rigid body with single contact point tire, and one DOF of relative motion with respect to the lower front assembly (rotation).

- *Swingarm*, composed of 3 rigid bodies (upper link, lower link, including transmission shaft, and wheel carrier). Kinematically, the swingarm represents a four-bar linkage, with one DOF of relative planar motion with respect to the main frame, describing the rear suspension travel. This can be inferred from Fig. 1, where the swingarm can be seen as a planar four-bar linkage, with 3 moving members with respect to the main frame, connected by 4 revolute joints.
- *Rear wheel*, including all rotating elements with the rear wheel, modeled as a single rigid body with single contact point tire, and one DOF of relative motion with respect to the rear wheel carrier (rotation).

At this stage, the flexibility of the 3 subsystems (main frame, front assembly, and swingarm) is introduced into the model by means of lumped stiffness elements. First, the front assembly and the swingarm are assumed to be "frozen" in a configuration of interest for the analysis. Then, each of the 3 subsystems is split into two rigid bodies connected by a fictitious revolute joint with a spring/damper element. This way, a (small) deformation of a flexible body is approximated by the relative (small) rotation between two rigid bodies about a deformation axis. Clearly, this requires the addition of 3 internal DOFs to the model, one for each flexible subsystem. Regarding the two bodies which compose the frame: one has the steering head joint, and the other provides the attachment point for the swingarm and longitudinal arm of the front assembly. For the front assembly and swingarm, the flexibility of the lumped stiffness model is obtained by introducing a massless body attached to the wheel carrier through the revolute joint associated with the lumped stiffness model. The wheel is then attached with the rotational DOF to the massless body itself. This way, the effect of flexibility on the wheel movement is reproduced.

For simulations, the open-source multibody simulation software MBSim [30] is used. The model order reduction needed for EMBS is carried out in Python with a code based on [31]; see [11] for further details.

4.2 Identification method

In this section, an identification method for lumped stiffness models is proposed aimed at representing with sufficient accuracy the effect of structural flexibility on weave and wobble. The basic procedure to create a lumped stiffness model starting from a single elastic body consists of splitting the body into two rigid bodies connected by a revolute joint. A rotational spring/damper is then associated with that joint. This way, a continuous (small) deformation of the elastic body is approximated by the relative rotation of two rigid bodies about a deformation axis. This approximation procedure needs to identify several parameters: the location and orientation of the revolute joint, the rotational stiffness and damping, and the inertia associated with each of the two bodies.

The adopted identification procedure, similar to that presented in [22–24], is described here referring to the simple case of a beam, as presented in Fig. 2. At one end of the undeformed beam, a reference system $O; x, y, z$ is fixed so that the axis of the beam lays in the plane (x, z). At the opposite end of the beam, another reference system $O'; x', y', z'$ is fixed so that x' and z' are parallel to x and z, respectively. It is now assumed that the beam is clamped at point O and free at point O'. An external load F_y is applied at point O' in y direction, causing a small displacement, which moves the point from position $\boldsymbol{q}_0$ to position $\boldsymbol{q}$. In general, this also produces a small rotation of the reference system fixed at point O'. Therefore, under the effect of the external load, the planes defined by (x, z) and (x', z') are no longer parallel. Their intersection identifies the deformation axis, which can be adopted

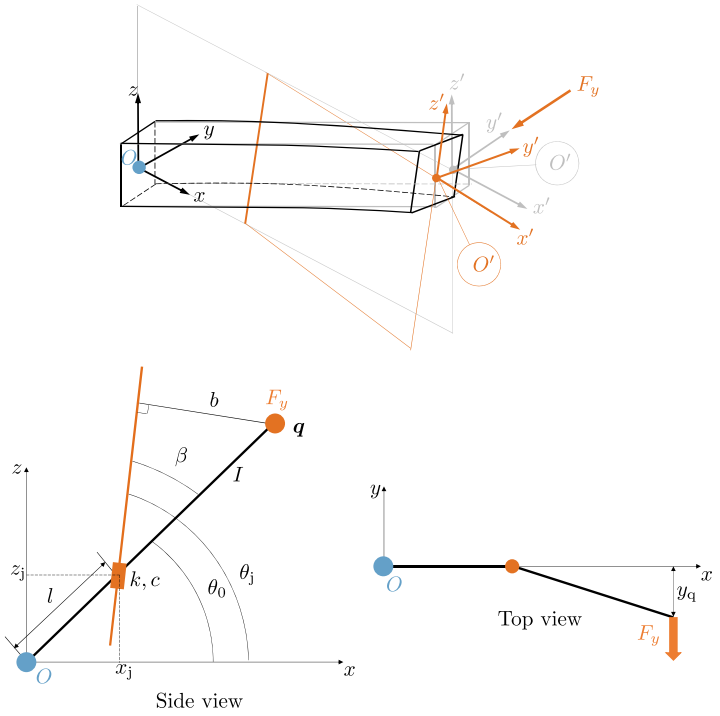

Fig. 2 Deformation axis of a beam cantilevered at the origin O (light blue dot) and having the load F applied to the free end (orange dot). (Color figure online)

for approximating the small deflection of the beam by means of the relative rotation of two rigid bodies.

Three types of tests are used: quasi-static test, harmonic test, and eigenvalue analysis. In the quasi-static test, a force is applied slowly so that the dynamics of the component is not excited. For the harmonic test, the load is applied with a sinusoidal wave oscillation, where the excitation frequency is constant throughout the test. In the eigenvalue analysis, the first bending and torsional eigenmodes and the related eigenvalues are identified. The amplitude of the forces applied to the components has been determined considering the loads that the components will experience during typical driving conditions, where the deformations remain in the linear range.

Based on these concepts, the procedure for identification of the lumped stiffness parameters shown in Fig. 2 can be defined. The explanation is divided into two parts: the identification of the geometric parameters l, β, b and the identification of stiffness k, damping c and vibrating inertia J.

The tests are carried out with simulations where the frame, front assembly, and swingarm are modeled with the same flexible bodies used for the motorcycle model in [11]. The measurements needed for the tests are provided by the simulation software itself.

4.2.1 Identification of l, β, b

The geometric parameters can be calculated either with static or harmonic tests. Define $\boldsymbol{q} = [x_q, y_q, z_q]$ the position of the free end and $\boldsymbol{R}$ its orientation matrix with respect to the

fixed inertial frame. With the static test, these values are measured after the quasi-static load has reached its maximum, while, during the harmonic test, the values from peak displacement are used.

The deformed plane is represented by $a_1x + a_2y + a_3z + a_4 = 0$. $\boldsymbol{n} = [a_1, a_2, a_3]$ is the vector perpendicular to the displaced plane of symmetry. As in Fig. 2, the plane of symmetry of the component is the x-z plane, and the vector is equal to the second column of matrix $\boldsymbol{R}$: $\boldsymbol{n} = \boldsymbol{R}_y$. Knowing the vectors $\boldsymbol{n}$ and $\boldsymbol{q}$, the coefficient a_4 of the plane equation can be determined:

$$a_4 = -(a_1 x_\mathrm{q} + a_2 y_\mathrm{q} + a_3 z_\mathrm{q}). \tag{1}$$

With the assumption that the plane of symmetry of the component under the test is the x-z plane, the position of the revolute joint can be found, see orange rectangle in Fig. 2. It could lay at any point along the deformation axis in Fig. 2. In this work, the revolute joint is placed at the intersection between the deformation axis and the line joining the origin of the inertial frame and the position $\boldsymbol{q}_0 = [x_{\mathrm{q}_0}, y_{\mathrm{q}_0}, z_{\mathrm{q}_0}]$ of the loaded end in its unloaded configuration. This line has the equation $z = \frac{z_{\mathrm{q}_0}}{x_{\mathrm{q}_0}} x$. Substituting $y = 0$ in the equation of the plane gives the equation of the deformation axis:

$$z = -\frac{a_1}{a_3} x - \frac{a_4}{a_3}. \tag{2}$$

The x coordinate x_j of the revolute joint can be calculated by substituting $z = \frac{z_{\mathrm{q}_0}}{x_{\mathrm{q}_0}} x$ in Equation (2):

$$x_\mathrm{j} = -\frac{a_4}{a_1 + a_3 \frac{z_{\mathrm{q}_0}}{x_{\mathrm{q}_0}}}. \tag{3}$$

The coordinate z_j is then automatically determined:

$$z_\mathrm{j} = \frac{z_{\mathrm{q}_0}}{x_{\mathrm{q}_0}} x_\mathrm{j}. \tag{4}$$

With these coordinates, the parameter l can be calculated:

$$l = \cos\left(\operatorname{atan}\left(\frac{z_\mathrm{j}}{x_\mathrm{j}}\right) - \operatorname{atan}\left(\frac{z_{\mathrm{q}_0}}{x_{\mathrm{q}_0}}\right)\right) \sqrt{x_\mathrm{j}^2 + z_\mathrm{j}^2}. \tag{5}$$

The cosine term is needed to determine if the revolute joint is at the positive or negative side of the x axis.

The angle β is calculated as difference between two angles:

$$\beta = \operatorname{atan}\left(-\frac{a_1}{a_3}\right) - \operatorname{atan}\left(\frac{z_{\mathrm{q}_0}}{x_{\mathrm{q}_0}}\right) = \theta_\mathrm{j} - \theta_0. \tag{6}$$

The angle β is wrapped between 0 and π, since the orientation of the revolute joint is insensitive to rotations of π. In fact, a rotational spring/damper element is assigned to the revolute joint, which acts equally in both directions of rotation.

Finally, the calculation of the moment arm b is given as:

$$b = (L - l)\sin\beta, \tag{7}$$

where $L = \sqrt{x_{q_0}^2 + z_{q_0}^2}$ is the distance between loaded end and the origin in the unloaded configuration.

The harmonic test provides one set of parameter l, β, b for every peak. The lumped stiffness model is then parameterized by the mean over these sets. In particular, the excitation is applied until the mean settles within a specified tolerance band.

4.2.2 Identification of k, c, J

The rotational stiffness k can be calculated by dividing the moment of the force F about the deformation axis by the rotation of the free end about the axis itself:

$$k = \frac{F_{st} \cdot b}{\operatorname{asin}\left(\frac{y_{q_{st}}}{b}\right)}, \tag{8}$$

where F_{st} and $y_{q_{st}}$ are the values of force amplitude and related displacement from a static test. b is the moment arm resulting either from the static or harmonic test, depending on the test chosen for identifying the geometric parameters in Sect. 4.2.1.

For the identification of c and J a different approach based on the eigenvalue analysis of each flexible body model is used. After identifying the first bending and torsional eigenmodes and under the assumption that they are sufficiently decoupled, the related eigenvalues are calculated. For underdamped systems, as it is the case for structural components, these can be expressed in the form:

$$\lambda_{1,2} = -\zeta_n \omega_n \pm j\omega_n \sqrt{1 - \zeta_n^2}, \tag{9}$$

where ω_n is the modal natural frequency, and ζ_n is the modal damping ratio. Note that Equation (9) is valid under the assumption of proportional viscous damping, which is acceptable in the case under analysis due to small amounts of structural damping. The imaginary part of Equation (9) provides the damped modal eigenfrequency ω_d. The modal natural frequency ω_n can be obtained from numerical simulation without damping or as the modulus of the eigenvalues $\lambda_{1,2}$ in Equation (9). Knowing ω_n and ω_d, the modal damping ratio ζ_n can be calculated. At this point, the modal inertia J and the damping c result from:

$$J = \frac{k}{\omega_n^2}, \tag{10}$$

$$c = 2\zeta_n J \omega_n. \tag{11}$$

This yields J and c for each of the two eigenmodes. Under the assumption of viscous damping, c can be directly used in the rotational spring damper element associated with the revolute joint.

4.2.3 Stiffness decomposition

For the sensitivity analysis in Sect. 4.3, two separated parameters for the bending and torsional stiffnesses are needed. However, the static test identifies only one stiffness value. The authors of [24] propose a method to split the stiffness identified with a static test between the deformation axes corresponding to the bending and torsion axes. Instead of only one revolute joint, the resulting lumped stiffness model has two revolute joints with rotation axes having the same directions of the bending and torsion axes. This concept is shown in

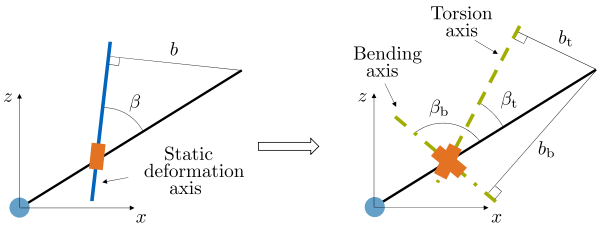

Fig. 3 Schematic representation of the stiffness decomposition: the stiffness about the static deformation axis is split into two stiffnesses about the bending and torsion axes

Fig. 3. This way, two stiffness parameters are available, but the overall flexural behavior of the lumped stiffness model is the same as that parameterized with just one revolute joint.

In the following, the procedure described in [24] is briefly summarized. Three tests with the component are needed: static test to identify the stiffness k, orientation β, and arm b; a harmonic test with the first bending eigenfrequency to identify the orientation β_b and arm b_b; and a harmonic test with the first torsional eigenfrequency to identify the orientation β_t and arm b_t. The unknowns are the stiffnesses about the bending axis k_b and torsion axis k_t. For the following two equations, two assumptions are made [24]: the displacement of the loaded end due to rotation about the static deformation axis is equal to the sum of the displacements due to rotations about bending and torsion axes, and the rotation about the static deformation axis of the loaded end is equal to the sum of the rotations about the bending and torsion axes. Additionally, as explained in [24], the assumption of small rotations is made. This makes it possible to consider the resultant rotation as the vector sum of components, where the order in which the rotations are performed is irrelevant. The adopted computational procedure is taken from [24]. The two unknowns k_b, k_t can be found by solving the system of equations:

$$\frac{b^2}{k} = \frac{b_b^2}{k_b} + \frac{b_t^2}{k_t}, \tag{12a}$$

$$\tan\beta = \frac{\frac{b_b}{k_b}\sin\beta_b + \frac{b_t}{k_t}\sin\beta_t}{\frac{b_b}{k_b}\cos\beta_b + \frac{b_t}{k_t}\cos\beta_t}. \tag{12b}$$

4.3 Sensitivity analysis

As explained in Sect. 3, the aim of the sensitivity analysis is to investigate the separated influence on weave and wobble of bending and torsional flexibility of each structural component on weave and wobble. The framework to carry out this analysis is provided by [25–27]. Basically, the influence of varying the stiffness parameters (main factors) on the damping of weave and wobble is analyzed. The procedure can be divided into three steps:

1. Definition of a stability index for weave and wobble.
2. Calculation of analysis of variance (ANOVA) to understand if there are interactions between the main factors.
3. If the interactions between the main factors are negligible, a linear correlation coefficient can be used (Pearson correlation coefficient) to show if an increase in the main factors, i.e., the stiffness parameters, leads to an increase or decrease in the stability index.

Starting from a plot of the real part of the eigenvalue of weave and wobble over longitudinal speed, the following two situations shown in Fig. 4 can be distinguished:

- The stability boundary is never crossed in the considered speed range, i.e. the real part of the eigenmode is negative at each speed. In this case, the stability index is defined as

minimum distance between the curve of the real part and the stability boundary:

$$s_1 = \max(\mathrm{Re}(\lambda)). \tag{13}$$

- The stability boundary is crossed at least once, i.e. its real part becomes positive. In this case, the stability index is defined as the ratio between the velocity range where the mode is stable and the whole velocity range considered:

$$s_2 = \frac{\|\boldsymbol{v}_{\text{stable}}\|}{v_{\max} - v_{\min}}, \tag{14}$$

where $\boldsymbol{v}_{\text{stable}}$ represents the interval of velocities where the mode is stable, see the thick segments in Fig. 4. In the case shown in Fig. 4, $\|\boldsymbol{v}_{\text{stable}}\| = (v_1 - v_{\min}) + (v_{\max} - v_2)$, where v_1 and v_2 are the points of the first and second roots, respectively. Depending on the shape of the curve, another calculation may be necessary, but the meaning of the index s_2 does not change. If there is only one root, only one interval for $\|\boldsymbol{v}_{\text{stable}}\|$ is identified. No more than two crossings are expected when studying weave and wobble as a function of the speed.

With reference to Fig. 4, it can be seen that the stability index s_2 is defined relatively to the whole interval of velocities achievable by the motorcycle. If the motorcycle is unstable in the whole velocity range, then $s_2 = 0$ (minimum stability, given by the fact that one or more eigenvalues have always positive real part in the whole velocity range). If the motorcycle is stable in the whole velocity range, then $s_2 = 1$ (maximum stability, given by the fact that one eigenvalue is at the stability threshold, with zero real part).

Equations (13) and (14) can be combined into a single stability index s:

$$s = \|\min(0, s_1)\| + s_2. \tag{15}$$

When the real part of the eigenvalue is always negative, $s_2 = 1$ and $s > 1$. If the stability boundary is reached, the first part of Equation (15) is zero, as s_1 is positive, and the index s varies between 0, which means that the eigenmode is unstable in the whole speed range, and 1, which indicates that the curve of the real part touches the stability boundary but never crosses it.

In the present work, the stability index is defined separately for low (40-100 km h^{-1}) and high (100-210 km h^{-1}) speeds. This covers all the relevant speeds up to the maximal speed of the motorcycle considered; speeds lower than 40 km h^{-1} are not relevant for studying weave and wobble in motorcycles. The distinction of the speed ranges is necessary, particularly for wobble, because parameters, such as the fork bending stiffness, act oppositely at a low and high speed [5–8]. The use of a single index for the whole speed range would fail to capture this distinction, thus falsifying the sensitivity analysis.

Similarly to [25–27], a full factorial design with two levels is chosen for an ANOVA with the stability index as response variable. The nominal values identified with the procedure in 4.2.3 are varied by ±10%. There are two stiffness values for each of the three considered structural components; this way, $2^6 = 64$ combinations are tested. After this analysis, it can be recognized if the variability of the six main factors is dominant, or if the interactions between them have a nonnegligible importance. The ANOVA is carried out with the `anovan` function of MATLAB.

Finally, if the interactions between the main factors are negligible, Doria [25] proposes to use the Pearson correlation coefficient to determine the effect of each factor, evaluated at the two levels, on the stability index. Using the same nomenclature as in [25], the Pearson

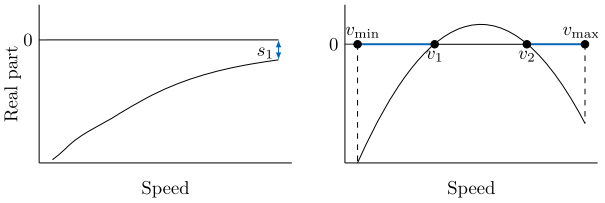

Fig. 4 Representation of stability indexes. Left: no crossing of the stability boundary, the index in Equation (13) is used. Right: two crossings of the stability boundary, the index in Equation (14) is used

correlation coefficient is ρ_{IF}, where F is the factor (stiffness), and I is the index (weave or wobble stability index), and it is defined as follows:

$$\rho_{IF} = \frac{\sigma_{IF}}{\sigma_I \sigma_F}. \tag{16}$$

σ_I, σ_F, σ_{IF} are, respectively, the variance of the index, the variance of each factor, and the covariance between index and factor:

$$\begin{aligned} \sigma_I^2 &= \frac{1}{n}\sum_{i=1}^{n}(I_i - \overline{I})^2, \\ \sigma_F^2 &= \frac{1}{n}\sum_{i=1}^{n}(F_i - \overline{F})^2, \\ \sigma_{IF}^2 &= \frac{1}{n}\sum_{i=1}^{n}(I_i - \overline{I})(F_i - \overline{F}), \end{aligned} \tag{17}$$

where n is the number of combinations of the factors, 64 in this case.

A value of ρ_{IF} close to 1 or -1 indicates either positive or negative strong correlation of the index I to the factor F [32].

5 Results

This section is divided into three subsections. Section 5.1 shows the results of the identification method presented in Sect. 4.2. In particular, the deformation axes of every structural component identified with static and harmonic tests are visualized. In Sect. 5.2, the accuracy in the simulation of weave and wobble of the lumped stiffness models with identified parameters is evaluated by comparing the results with the flexible multibody motorcycle model. Section 5.3 presents the results of the sensitivity analysis.

5.1 Results of parameter identification

The deciding point when identifying the lumped stiffness parameters is to pick the right load combination. In fact, as presented in [22, 23], static and harmonic loads identify different parameters. Figures 5, 6, and 7 show the deformation axes for every structural component with the static and harmonic test. The x axis represents the longitudinal axis of the motorcycle, and the z axis points upwards. The blue line is the deformation axis identified with the static test. The two green lines are the deformation axes resulting from harmonic tests having the frequency of the first bending and torsional eigenmodes, named bending and torsion axes. Table 1 shows the first torsional and bending eigenfrequencies for each component.

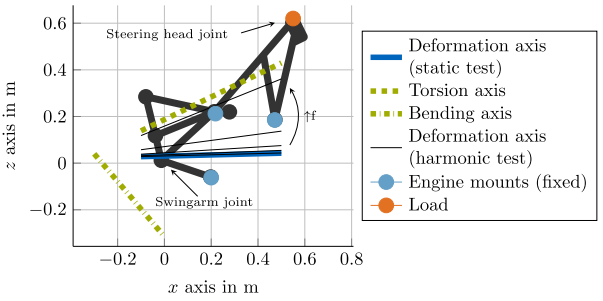

Fig. 5 Visualization of deformation axes of the frame with different loads. The component is fixed at the engine mounts and the load is applied to the steering head joint. (Color figure online)

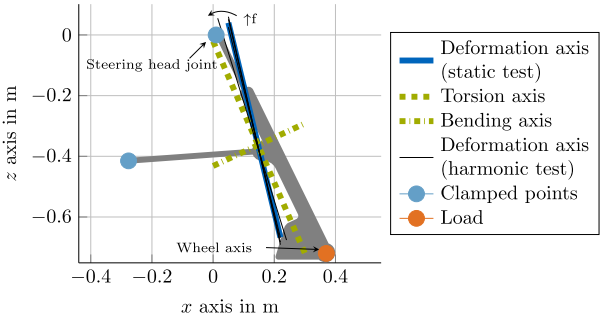

Fig. 6 Visualization of deformation axes of the front assembly with different loads. The component is clamped at the steering head joint and at the revolute joint of the longitudinal arm. The load is applied to the wheel axis. (Color figure online)

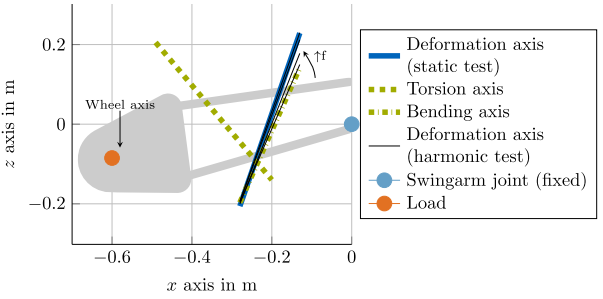

Fig. 7 Visualization of deformation axes of the swingarm with different loads. The component is fixed at the swingarm joint and the load is applied to the wheel axis. (Color figure online)

Table 1 First torsional and bending eigenfrequency of frame, front assembly, and swingarm

Component	Eigenfrequency	Mode shape
Frame	74 Hz	Torsion
	93 Hz	Bending
Front assembly	28 Hz	Torsion
	79 Hz	Bending
Swingarm	112 Hz	Bending
	321 Hz	Torsion

The black thin lines show the deformation axes when the excitation frequency of the harmonic test is varied from 1 Hz to a frequency of 5 Hz below the first eigenfrequency of the component. Similarly to Fig. 2, the light blue dots are the points where the component is fixed to the inertial frame, and the orange dots are the points where the load is applied.

In Fig. 5, the frame is fixed at the engine mounts, and the load is applied to the steering head joint. The choice of fixing the engine mounts allows the consideration of the contribution of the engine to the overall stiffness. In fact, in the motorcycle, the frame is mounted on the engine itself, which is assumed rigid in this paper. The eigenfrequencies in Table 1 are obtained with the tank and saddle mounted on the frame and modeled as rigid bodies with mass and inertia. The torsion axis is nearly parallel to the line joining the swingarm joint and the steering head joint, where the load is applied. The bending axis is nearly perpendicular to the torsion axis and lays behind the swingarm joint, signalizing that, when oscillating with the first bending eigenmode, the steering head joint mainly translates along the y axis, i.e. in the direction orthogonal to the symmetry plane of the frame. The static deformation axis is a combination of torsion and bending; this is due to the fact that the frequencies of the first torsion and bending eigenfrequencies are close in value. As expected, by sweeping the frequency of the harmonic excitation, the deformation axis moves from the static deformation axis to the deformation axis of the first eigenmode, i.e., the torsion axis.

The front assembly is clamped at the steering head joint and at the joint between the longitudinal arm and the frame to avoid the movement of the suspension (Fig. 6). The load is applied at the wheel axis. The longitudinal arm of the multilink suspension is also shown. The torsion axis is, as expected, nearly parallel to the fork axis, while the bending axis is almost perpendicular to it. Also, in this case, the static deformation axis is a combination of torsion and bending. However, torsion dominates the deformation of the assembly for a static excitation because the eigenmode with the lowest eigenfrequency is torsional, and the frequency of the first bending eigenmode is significantly higher (Table 1). This is different from conventional forks that generally have lower bending stiffness than torsional stiffness [22]. The high bending stiffness in the present case can be attributed to the presence of the longitudinal arm. The harmonic test with increasing frequency (black lines in Fig. 6) identifies a deformation axis that progressively moves from the static axis to the axis of the eigenmode.

The swingarm, Fig. 7, is fixed at the joint with the frame, and the force is applied to the wheel axis. As mentioned in Sect. 4.1, it is a four-bar link composed of a lower link, upper link, and wheel carrier. Unlike frame and front assembly, the first eigenmode is a bending one, see Table 1. The bending axis is, as expected, almost perpendicular to the main arm and link, and the torsion axis is nearly perpendicular to the bending axis. The static deformation axis is dominated by bending because it is the first eigenmode, and the first torsional eigenmode has a significantly higher eigenfrequency. Also, in this case, when increasing the frequency of the harmonic test, the deformation axis moves from the static axis to the axis of the first eigenmode.

When building the lumped stiffness model of a structural component, the single body must be split into two bodies. Regarding the frame, the inertia of the body to which the handlebar is attached is the one identified through the test in Sect. 4.2.2. The mass of the frame, engine, tank, and saddle is concentrated into the other body to which the swingarm and the longitudinal arm of the front assembly are connected; the inertia of this body is calculated such that the overall inertia of the motorcycle remains the same. For the front assembly and swingarm, the identified inertia is assigned to the massless body used for the lumped stiffness model, see Sect. 4.1. Inertia must then be removed to ensure that the overall inertia remains constant. In the case of the front assembly, this inertia is removed from the lower fork, while for the swingarm, the inertia is removed from the wheel carrier.

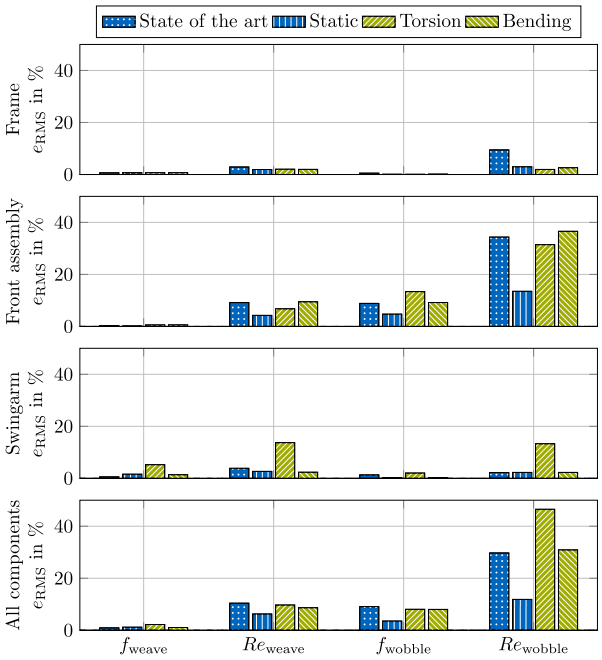

Fig. 8 Root mean square error in percentage of lumped stiffness models compared to the flexible multibody models

5.2 Accuracy of identified lumped stiffness models

At this point, the accuracy of lumped stiffness models in simulating the influence of flexibilities on weave and wobble is investigated. For that, the models are compared to the flexible multibody motorcycle model presented in [11], which is considered the "ground truth". In particular, the eigenfrequency f and real part Re of weave and wobble are determined between 40 and 210 km h^{-1}, and the root mean square error in percentage between the lumped stiffness models and the flexible body models is calculated:

$$e_{\mathrm{RMS}_{\%}} = \frac{\sqrt{\frac{1}{N}\sum_{i=1}^{N}(x_{\mathrm{lu}} - x_{\mathrm{fl}})^2}}{\bar{x}_{\mathrm{fl}}} \cdot 100. \tag{18}$$

N is the number of speed values for which weave and wobble are simulated. x_{lu}, x_{fl} are either the frequency or the real part of weave or wobble calculated with the lumped stiffness and flexible body model, respectively. $\bar{x}_{\mathrm{fl}}$ is the mean over the speed range of either frequency or real part calculated with the flexible body model.

The results are shown with the bar diagram in Fig. 8. In the first three plots, the frame, front assembly, and swingarm are studied separately: for each case, only the flexibility of that component is included in the motorcycle model, with either lumped stiffness or flexible multibody approach. The last plot represents the case where the flexibility of all structural components is modeled simultaneously. Different lumped stiffness models are shown in Fig. 8. The one marked with "State of the art" uses the common assumptions found in the literature for the orientation of the revolute joints; moreover, the stiffness values are measured with static tests on the flexible multibody model of each structural component. The case marked with "Static" uses the identification procedure of Sect. 4.2 with the quasi-static

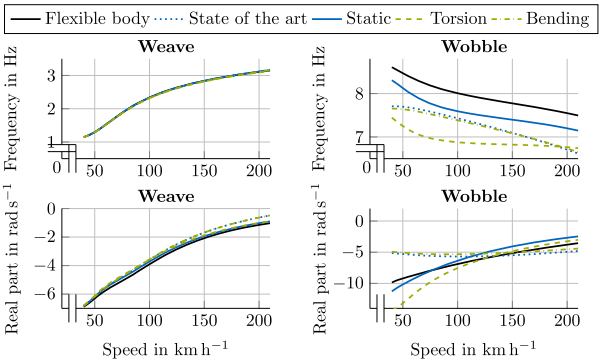

Fig. 9 Effect of the flexibility of the front assembly on weave and wobble (only the flexibility of the front assembly is modeled): comparison between flexible body, state-of-the-art lumped stiffness, and lumped stiffness models parameterized with the procedure in Sect. 4.2

application of the load. The bars marked with "Torsion" and "Bending" also use the identification procedure but with harmonic tests at the frequency of the first torsional and bending eigenmodes of the flexible body, respectively. "State of the art" and "Static" lumped stiffness models are obtained with a static test because they approximate the response of the component to static loads; for this reason, they both do not use the identified inertia. In contrast, "Torsion" and "Bending" lumped stiffness models approximate the frequency response of the component at the first torsional and bending eigenfrequencies. For this reason, Equation (10) is applied to the first torsional and bending eigenfrequencies, thus obtaining the modal inertia about the torsional and bending axes, respectively. The distribution of the inertia is done as explained at the end of Sect. 5.1.

Figure 8 does not show the error of lumped stiffness models parameterized with harmonic tests with a frequency below the first eigenfrequency of the flexible component because their results are similar to the lumped stiffness models parameterized either with the static test or harmonic test at the first eigenfrequency. In particular, for frequencies up to 10-20 Hz lower than the first eigenfrequency, the static test and the harmonic test identify very similar parameters (see Figs. 5, 6, and 7), and, therefore, the resulting lumped stiffness models are equivalent. In the rest of this section, the accuracy of the lumped stiffness models of the structural components is analyzed separately.

5.2.1 Frame

The "State of the art" lumped stiffness model of the frame represents the frame torsion with a revolute joint at the steering head joint with a rotation axis perpendicular to the fork axis [5]; the front assembly is then attached to that joint. In the present paper, the related stiffness is measured with a static moment applied to the steering head joint and perpendicular to the fork axis. As the frame of the present motorcycle is very stiff, all lumped stiffness models show low error in almost all cases. However, the "State of the art" model presents a relatively high error in the real part of the wobble eigenvalue, whereas the lumped stiffness models with parameters identified by the procedure in the present work perform significantly better. In particular, it has been verified that the "State of the art" model shows an eigenvalue with smaller real part (in modulus) at high speed than the "ground truth", which signifies the stiffness is too high, see, e.g., [5–7].

5.2.2 Front assembly

The state-of-the-art approach for modeling the bending flexibility of the front assembly is to put a revolute joint with a rotation axis perpendicular to the fork axis. The related stiffness is

measured with a static lateral force applied to the wheel axis, see [11]. The revolute joint is located at the position of the spherical joint of the longitudinal arm, see [11] for more details on this decision. For the "State of the art" and "Static" lumped stiffness models, it has been verified that it is important that the inertia of the lower fork is activated during the motion of the wheel due to flexibility. For this reason, the inertia of the lower fork is moved to the massless body used for the definition of the lumped stiffness model while ensuring that the position of the center of gravity is not changed. In the "Torsion" and "Bending" lumped stiffness models, instead, the identified modal inertia is assigned to the massless body to correctly represent the frequency response of the component at the first bending and torsion eigenfrequencies. The front assembly is the component where the lumped stiffness models have the highest error, in particular in the real part of wobble. For this reason, it is worth looking in more detail at the evolution of weave and wobble with speed, shown in Fig. 9. The plots clarify that the "Static" lumped stiffness model provides the best approximation of the "ground truth", i.e., the flexible multibody model. Interestingly, the "State of the art" lumped stiffness model and the "Bending" lumped stiffness model provide very similar results. This is due to the fact that the bending axis is almost perpendicular to the fork axis, see Fig. 6, and the resulting lumped stiffness model is therefore very similar to the "State of the art" model. This configuration, however, does not accurately represents the deformation of the front assembly when simulating weave and wobble.

5.2.3 Swingarm

For the swingarm, there is no general trend in the state-of-the-art. For this reason, the "State of the art" model here represents a possible simplified modeling approach for simulating the swingarm torsion: a revolute joint with a rotation axis parallel to the vehicle x axis (longitudinal axis) is put between the wheel center and the wheel carrier, see for example [33]. The related stiffness derives from a static test where a moment parallel to the vehicle x axis is applied to the wheel axis. The swingarm of the present motorcycle model has high stiffness, and, therefore, the differences between the models are small. The "Static" lumped stiffness model has the lowest error. In contrast, the "Torsion" lumped stiffness model shows a high error.

5.2.4 All components

The same considerations made above apply to the case where the flexibility of all structural components is modeled simultaneously: the largest error is in the real part of the wobble eigenmode, whereby the lumped stiffness models parameterized with the static test only show an error of at most 10%, thus overperforming the other lumped stiffness models.

In summary, the "Static" lumped stiffness models show the smallest error for every structural component and they offer a relevant improvement in accuracy compared to the state-of-the-art. The "Torsion" and "Bending" lumped stiffness models have higher errors than the "Static" lumped stiffness model so that the static test seems the best approach for parameterizing lumped stiffness models having the aim of modeling weave and wobble.

It is worth pointing out that the damping and inertia parameters identified through Equation (10) and (11) have a minor influence on weave and wobble. The main parameters influencing the stability of the two eigenmodes are the stiffness and location of the revolute joint. This is the reason why, for the lumped stiffness model identified with the static test, a very small value of damping is used. It can be calculated by multiplying the identified rotational stiffness by the proportionality constant $\gamma = 0.001$ s, thus obtaining $c = \gamma k$.

Table 2 Nominal values of stiffness about the static deformation axis k and stiffness about the torsion k_t and bending k_b axis after decomposition with the method in Sect. 4.2.3

	k in N m rad^{-1}	k_t in N m rad^{-1}	k_b in N m rad^{-1}
Frame	$1.03{\cdot}10^6$	$3.75{\cdot}10^5$	$3.59{\cdot}10^6$
Front assembly	$1.06{\cdot}10^4$	$5.95{\cdot}10^3$	$1.71{\cdot}10^5$
Swingarm	$1.33{\cdot}10^5$	$1.04{\cdot}10^6$	$1.39{\cdot}10^5$

5.3 Sensitivity analysis

In this section, a sensitivity analysis is carried out to answer the question of which stiffness within each component has the highest impact on the stability of weave and wobble. The stability index defined in Sect. 4.3 is used. Two separated analyses are done for the low speeds (40-100 km h^{-1}) and high speeds (100-210 km h^{-1}). This allows for the identification of the stiffness parameters that have opposite effects according to the speed range considered.

Once the parameters for the static deformation axis of each structural component are identified in Sect. 5.1, the stiffness about that axis is split along the torsion and bending axes with the procedure in Sect. 4.2.3. Table 2 presents these values for every structural component. The obtained stiffness values about torsion and bending axes are then varied in the range $\pm 10\%$, and the stability indexes for each of the 64 combinations are calculated.

First of all, the ANOVA is carried out to check which percentage of the variability of the stability index is due to main effects and how much depends on interactions between factors. For each stability index, approximately 99% of the variability is due to main factors. Therefore, the evaluation with the Pearson correlation coefficient is possible.

It has been verified that, for the motorcycle considered and for any combination of the lumped stiffness parameters, weave and wobble never cross the stability boundary, so only the stability index in Equation (13) is used.

Fig. 10 shows the Pearson correlation coefficients for every stiffness and distinguishes between weave and wobble. The subscript used must be interpreted as follows: the first letter indicates the type of flexibility (t for torsion and b for bending), and the second letter indicates the structural component (f is the frame, a is the front assembly, and s is the swingarm). A positive correlation coefficient means that an increase in the considered stiffness leads to increased damping of the mode.

The bar plot of wobble makes it clear why this analysis was conducted separately for the low- and high-speed ranges. There are stiffness parameters, such as torsional and bending stiffness of the frame and bending stiffness of the front assembly, that oppositely contribute to the two speed ranges.

At this point, some considerations about a stability-optimized design of structural components can be made. The following is valid for the present structural components and the shown nominal stiffness values; the extension to components with other designs can be a further research topic. High-frame torsional and bending stiffnesses have positive effects on the high-speed weave and low-speed wobble but a slightly negative effect on the high-speed wobble, which overlaps with experimental tests carried out in [34]. The front assembly is the part whose stiffness has the strongest effect on both eigenmodes. Too high torsional stiffness should be avoided because it destabilizes wobble at every speed and has only a small stabilizing effect on weave. Finding the optimal value of bending stiffness is a tricky task: on the one hand, the high bending stiffness of front assembly stabilizes the high-speed weave and the low-speed wobble; on the other hand, it strongly destabilizes the high-speed wobble. This stiffness should be therefore designed considering the characteristics of the whole motorcycle, such as its overall geometry and weight distribution, tire properties and

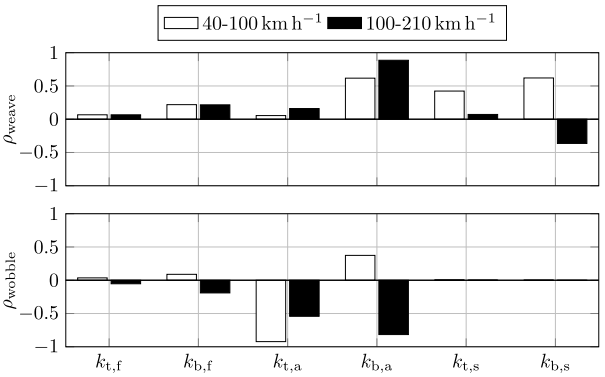

Fig. 10 Pearson correlation coefficients of weave and wobble for every structural stiffness

the presence of a steering damper. Please note that the torsion axis of the frame and the bending axis of the front assembly have similar orientation, see Fig. 5 and 6. In fact, they produce qualitatively similar results. The smaller sensitivity of the frame torsion is due to two effects: its nominal value is very high, so even with a variation of 10%, the stiffness always remains high; the front assembly bending flexibility directly affects the motion of the front wheel, while the frame torsional flexibility does that indirectly through the motion of the front assembly, which in the present case is also affected by the presence of the longitudinal arm. The swingarm stiffness hardly affects wobble, which is mainly influenced by the parameters of the motorcycle's front. Reducing swingarm bending stiffness brings positive effects to the high-speed weave but negative effects to the low-speed weave. However, weave is never critical at low speed, so an optimized design for the investigated configuration of the swingarm would involve relatively low bending stiffness but high torsional stiffness.

Of course, when reducing the stiffness of structural components with the aim of saving weight, the effects on driving dynamics as a whole and strength requirements must also be taken into account.

6 Conclusions

This paper proposes a method for parameterizing lumped stiffness models of motorcycle structural components. For that, static and harmonic tests are carried out in simulations with the components modeled as flexible bodies.

The main objective is to evaluate whether the lumped stiffness models parameterized with this method are accurate enough to simulate the influence of flexibilities on weave and wobble. The motorcycle model with lumped stiffnesses is therefore compared to the flexible multibody motorcycle model, which is considered "ground truth" because it has the most realistic modeling of flexibilities. The error of lumped stiffness models can be evaluated by simulating the frequency and real part of weave and wobble with these two models. Results show that the most suitable test for parameterizing lumped stiffness models with the aim of simulating weave and wobble is the static test. Moreover, the presented method for parameterization allows a significant improvement in accuracy compared to the state-of-the-art lumped stiffness models, which are generally based on assumptions for the position of the revolute joints used to model the flexibility.

It can be concluded that thanks to the presented method, lumped stiffness models reach enough accuracy to simulate the effect of flexibilities on weave and wobble. For modeling

phenomena with higher frequency, such as comfort tests, lumped stiffness model parameterized with harmonic tests at higher frequency could provide better results. However, there is also the possibility that, in these situations, only flexible multibody models provide sufficient accuracy thanks to their ability to reproduce frequency contents in a broad range.

The second main contribution of this work is the sensitivity analysis of component stiffnesses to point out which stiffness within each component has the highest impact on the stability and to make suggestions for an optimized design of structural components of the motorcycle model considered in this paper. The results stress the big influence of the flexibilities of the front assembly on both weave and wobble. Its torsional stiffness should not be too high to avoid the destabilization of wobble, while its bending stiffness should be optimized considering that a high value is advantageous for the high-speed weave damping and low-speed wobble damping but detrimental for the high-speed wobble damping. Finally, the flexibilities of swingarm only influence weave, and a stability-optimized design could involve relatively low bending stiffness but high torsional stiffness.

These considerations about possible optimal design are valid for the present components with the characteristics of the deformation axes provided. Literature shows that components with alternative constructions present different deformation characteristics, so the extension to other designs for the structural components could be a further research topic. The method presented in this paper is suitable for all types of structural components so that this extension can be easily carried out.

Appendix A

In this appendix, a summary of the information in [11] about the flexible multibody motorcycle model is reported.

As mentioned in Sect. 4.1, the following structural components of the motorcycle are modeled as flexible bodies:

- Frame, which is fixed to a rigid engine.
- Front assembly, which is composed of fork bridge, two stanchions, longitudinal arm, and lower fork.
- Swingarm, which is composed of lower link, upper link, and wheel carrier.

These bodies are initially modeled with FEM. However, they contain up to 10^6 degrees of freedom, so it would be impossible to directly include them in a multibody simulation environment because this would lead to unacceptable computation time. Therefore, model order reduction (MOR) is applied. In [11], the Craig-Bampton method is used, which has the peculiarity of distinguishing between the boundary and internal degrees of freedom. The boundary degrees of freedom serve as an attachment point for other bodies in an assembly or to apply external forces and are preserved by the reduction with the Craig-Bampton method. The internal degrees of freedom are reduced by applying modal truncation. In particular, the first 20 fixed-interface modes have been kept for each body. This way, the frequency content up to 600 Hz is included in the reduced order bodies. Table A.1 shows the degrees of freedom for each flexible body before and after MOR with Craig-Bampton. The degrees of freedom of the reduced order models are expressed as a sum to distinguish the number of boundary degrees of freedom (second number) from the number of selected modes.

For embedding the reduced order models of the structural components in the multibody simulation environment of the motorcycle, the Floating Frame of Reference Formulation is

Table A.1 Degrees of freedom of the flexible bodies before and after the model order reduction

		DOFs FEM	DOFs after MOR
Frame		$3{,}8{\cdot}10^6$	20+54
Front assembly	Fork bridge	$8{,}0{\cdot}10^5$	20+9
	Stanchions (each)	$2{,}1{\cdot}10^5$	20+9
	Lower fork	$1{,}7{\cdot}10^6$	20+18
	Longitudinal arm	$4{,}7{\cdot}10^5$	20+12
Swingarm	Lower link	$2{,}7{\cdot}10^6$	20+15
	Upper link	$4{,}1{\cdot}10^5$	20+6
	Wheel carrier	$2{,}1{\cdot}10^6$	20+12

used, which is suitable for describing the deformation of bodies that undergo small linear elastic displacement combined with big nonlinear rigid body motions.

The flexible multibody model of the frame and front assembly has been validated by comparing the stiffness resulting from static tests on the real components. In particular, the frame has been tested by clamping it at the swingarm axis and applying a lateral force at the steering head joint. The stiffness resulting from the flexible body deviates 6.4% from the experimental data. The front assembly is clamped at the steering head joint, and the lateral force is applied to the wheel axis. In this case, the error between experiment and simulation is 0.5%. The validation for the swingarm was not possible because no measurements were available.

Author contributions Francesco Passigato initiated the idea of the paper and contributed significantly to the concept, modeling, and results. Alexander Schramm made significant contributions in the development of methods and in the review phase. Silvio Sorrentino and Alessandro De Felice contributed to the review phase. Achim Gordner contributed to significant discussion of the results. Frank Diermeyer contributed to the whole concept of the paper. Frank Diermeyer gave final approval for publication of this version and is in agreement with all aspects of the work. As a guarantor, he accepts responsibility for the overall integrity of this paper.

Funding Open Access funding enabled and organized by Projekt DEAL. Francesco Passigato is funded by BMW Group (Germany).

Data Availability The model data belong to BMW Group and can therefore not be published.

Declarations

Ethical Approval Not applicable

Competing interests The authors declare no competing interests.

References

1. Cossalter, V., Lot, R., Maggio, F.: The modal analysis of a motorcycle in straight running and on a curve. Meccanica **39**, 1–16 (2004)
2. Cossalter, V.: Motorcycle Dynamics, 2. english edn. Lulu Press, S.l, Padova, Italy (2006)
3. Sharp, R.S., Limebeer, D.J.N.: A motorcycle model for stability and control analysis. Multibody Syst. Dyn. **6**, 123–142 (2001)
4. Sharp, R.S.: The stability and control of motorcycles. J. Mech. Eng. Sci. **13**(5), 316–329 (1971)
5. Sharp, R.S., Alstead, C.J.: The influence of structural flexibilities on the straight-running stability of motorcycles. Veh. Syst. Dyn. **9**(6), 327–357 (1980). https://doi.org/10.1080/00423118008968629
6. Spierings, P.T.J.: The effects of lateral front fork flexibility on the vibrational modes of straight-running single-track vehicles. Veh. Syst. Dyn. **10**(1), 21–35 (1981). https://doi.org/10.1080/00423118108968633
7. Cossalter, V., Lot, R., Massaro, M.: The influence of frame compliance and rider mobility on the scooter stability. Veh. Syst. Dyn. **45**(4), 313–326 (2007). https://doi.org/10.1080/00423110600976100
8. Passigato, F., Eisele, A., Wisselmann, D., Gordner, A., Diermeyer, F.: Analysis of the phenomena causing weave and wobble in two-wheelers. Appl. Sci. **10**(19), 6826 (2020). https://doi.org/10.3390/app10196826
9. Schwertassek, R., Wallrapp, O., Shabana, A.A.: Flexible multibody simulation and choice of shape functions. Nonlinear Dyn. **20**(4), 361–380 (1999)
10. Doria, A., Formentini, M.: Identification of the structural modes of high performance bicycles in the perspective of wobble control: parts a and b. In: Proceedings of the ASME Design Engineering Technical Conference, vol. 4, pp. 551–560 (2011). www.scopus.com
11. Passigato, F., Gordner, A., Diermeyer, F.: Modeling of the weave and wobble eigenmodes of motorcycles using flexible multibody simulation International Design Engineering Technical Conferences and Computers and Information in Engineering Conference, Vol 9: 18th International Conference on Multibody Systems, Nonlinear Dynamics, and Control (MSNDC) (2022). https://doi.org/10.1115/DETC2022-89945.
12. Koenen, C., Pacejka, H.B.: The influence of frame elasticity and simple rider body dynamics on free vibrations of motorcycles in curves. Veh. Syst. Dyn. **10**(2–3), 70–73 (1981). https://doi.org/10.1080/00423118108968637
13. Koenen, C.: The Dynamic Behaviour of a Motorcycle when Running Straight Ahead and when Cornering: Delft. Techn. Hogeschool, Proefschrift **1983** (1983)
14. Sharp, R.S.: Stability, control and steering responses of motorcycles. Veh. Syst. Dyn. **35**(4–5), 291–318 (2001). https://doi.org/10.1076/vesd.35.4.291.2042
15. Sharp, R.S., Evangelou, S., Limebeer, D.J.N.: Advances in the modelling of motorcycle dynamics. Multibody Syst. Dyn. **12**(3), 251–283 (2004)
16. Sharp, R.S., Limebeer, D.J.N.: On steering wobble oscillations of motorcycles. Proc. Inst. Mech. Eng., Part C, J. Mech. Eng. Sci. **218**(12), 1449–1456 (2004). https://doi.org/10.1243/0954406042690434
17. Evangelou, S., Limebeer, D.J.N., Sharp, R.S., Smith, M.C.: Mechanical steering compensators for high-performance motorcycles. Trans. ASME J. Appl. Mech. **74**(2), 332–346 (2007)
18. Evangelou, S., Limebeer, D.J.N., Tomas-Rodriguez, M.: Suppression of burst oscillation in racing motorcycle. J. Appl. Mech. **80** (2013)
19. Sharp, R.S., Watanabe, Y.: Chatter vibrations of high-performance motorcycles. Veh. Syst. Dyn. **51**(3), 393–404 (2013). https://doi.org/10.1080/00423114.2012.727440
20. Cossalter, V., Lot, R., Massaro, M.: An advanced multibody code for handling and stability analysis of motorcycles. Meccanica **46**(5), 943–958 (2011). https://doi.org/10.1007/s11012-010-9351-7
21. Doria, A., Favaron, V., Taraborrelli, L., Roa, S.: Parametric analysis of the stability of a bicycle taking into account geometrical, mass and compliance properties. Int. J. Veh. Des. **75**(1–4), 91–123 (2017)
22. Cossalter, V., Doria, A., Massaro, M., Taraborrelli, L.: Experimental and numerical investigation on the motorcycle front frame flexibility and its effect on stability. Mech. Syst. Signal Process. **60–61**, 452–471 (2015). https://doi.org/10.1016/j.ymssp.2015.02.011
23. Taraborrelli, L., Favaron, V., Doria, A.: The effect of swingarm stiffness on motorcycle stability: experimental measurements and numerical simulations. Int. J. Veh. Syst. Model. Test. **12**(3/4), 240 (2017). https://doi.org/10.1504/IJVSMT.2017.089981
24. Doria, A., Taraborrelli, L.: The twist axis of frames with particular application to motorcycles. Proc. Inst. Mech. Eng., Part C, J. Mech. Eng. Sci. **230**(17), 3026–3039 (2016). https://doi.org/10.1177/0954406215604862
25. Doria, A., Roa, S.: On the influence of tyre and structural properties on the stability of bicycles. Veh. Syst. Dyn. **56**(6), 947–966 (2018)
26. Doria, A., Roa, S., Muñoz, L.: Stability analysis of bicycles by means of analytical models with increasing complexity. Mech. Sci. **10**(1), 229–241 (2019). https://doi.org/10.5194/ms-10-229-2019

27. Roa, S., Doria, A., Muñoz, L.: Optimization of the bicycle weave and wobble modes. ASME **3** (2018). https://doi.org/10.1115/DETC2018-86132
28. Pacejka, H.B.: Tyre and Vehicle Dynamics, 2 edn. Elsevier Butterworth-Heinemann, Amsterdam and Heidelberg (2006)
29. BMW Group: the new BMW R 1200 GS. https://www.press.bmwgroup.com/global/article/detail/T0132324EN/the-new-bmw-r-1200-gs
30. Schindler, T., Förg, M., Friedrich, M., Schneider, M., Esefeld, B., Huber, R., Zandler, R., Ulbrich, H.: In: Analysing Dynamical Phenomenons: Introduction to mbsim. The 1st Joint International Conference on Multibody System Dynamics, 2010 May 25-27, Lappeenranta, Finland (2010)
31. Meyer, C.H., Lerch, C., Maierhofer, J.: AMfe. Chair of Applied Mechanics, Technical University of Munich. https://github.com/AppliedMechanics/AMfe
32. Schober, P., Boer, C., Schwarte, L.: Correlation coefficients: appropriate use and interpretation. Anesth. Analg. **126**(5), 1763–1768 (May 2018). https://doi.org/10.1213/ANE.0000000000002864
33. Dipl.-Ing. Dirk Wisselmann: Motorrad-Fahrdynamik-Simulation. Modellbildung, Validierung und Anwendung: PhD Thesis. VDI-Berichte, Dachau (1992)
34. Roe, G.E., Thorpe, T.E.: The influence of frame structure on the dynamics of motorcycles stability SAE Technical Papers (1989)